Dynamic Snap-Through of Thermally Buckled Structures by a Reduced Order Method

Adam Przekop*

National Institute of Aerospace, Hampton, VA 23666

Stephen A. Rizzi†

NASA Langley Research Center, Hampton, VA 23681

The goal of this investigation is to further develop nonlinear modal numerical simulation methods for application to geometrically nonlinear response of structures exposed to combined high intensity random pressure fluctuations and thermal loadings. The study is conducted on a flat aluminum beam, which permits a comparison of results obtained by a reduced-order analysis with those obtained from a numerically intensive simulation in physical degrees-of-freedom. A uniformly distributed thermal loading is first applied to investigate the dynamic instability associated with thermal buckling. A uniformly distributed random loading is added to investigate the combined thermal-acoustic response. In the latter case, three types of response characteristics are considered, namely: (i) small amplitude vibration around one of the two stable buckling equilibrium positions, (ii) intermittent snap-through response between the two equilibrium positions, and (iii) persistent snap-through response between the two equilibrium positions. For the reduced-order analysis, four categories of modal basis functions are identified including those having symmetric transverse, anti-symmetric transverse, symmetric in-plane, and anti-symmetric in-plane displacements. The effect of basis selection on the quality of results is investigated for the dynamic thermal buckling and combined thermal-acoustic response. It is found that despite symmetric geometry, loading, and boundary conditions, the anti-symmetric transverse and symmetric in-plane modes must be included in the basis as they participate in the snap-through behavior.

* Research Scientist, AIAA Senior Member.
† Aerospace Engineer, Structural Acoustics Branch, AIAA Associate Fellow.

Nomenclature

$\boldsymbol{M}, \tilde{\boldsymbol{M}}$ = mass matrix (physical and modal coordinates)

$\boldsymbol{C}, \tilde{\boldsymbol{C}}$ = proportional damping matrix (physical and modal coordinates)

$\boldsymbol{K}, \tilde{\boldsymbol{K}}$ = stiffness matrix (physical and modal coordinates)

$\boldsymbol{X}, \boldsymbol{q}$ = displacement response vector (physical and modal coordinates)

$\boldsymbol{F}, \tilde{\boldsymbol{F}}$ = force excitation vector (physical and modal coordinates)

$\boldsymbol{F}_{NL}, \tilde{\boldsymbol{F}}_{NL}$ = nonlinear restoring force (physical and modal coordinates)

$\boldsymbol{\Phi}$ = modal basis function matrix

u, v, ϕ = horizontal and vertical displacement, and rotation (global physical coordinates)

ΔT = temperature increment

t = time

d, a, b = linear, quadratic nonlinear, and cubic nonlinear modal stiffness coefficients

$\lceil \boldsymbol{I} \rfloor$ = identity matrix

α = thermal expansion coefficient

ζ = viscous damping factor

ω = undamped natural frequencies

I. Introduction

DIRECT numerical simulation of nonlinear random response in physical degrees-of-freedom (DoF) is computationally intensive even for the simplest structures. Its use for design of high-cycle-fatigue tolerant aerospace vehicle structures, requiring long simulation times to obtain meaningful statistics, is considered impractical. Accordingly, much effort has been spent in recent years to develop accurate reduced-order analyses, such as finite-element-based nonlinear modal numerical simulation, which could be suitable for use in design environments.

Aerospace structures exposed to a high-intensity random acoustic loading are often also simultaneously exposed to an elevated thermal environment.[1] Since both acoustic and thermal loadings can cause the structure to respond in

a geometrically nonlinear fashion, an analysis technique that permits simultaneous loading is required, i.e. linear superposition of the acoustic and thermal response is not suitable. Under certain thermal-acoustic loading conditions, experimental studies indicate a snap-though response,[2-4] which can significantly reduce fatigue life. The snap-through problem has previously been investigated using reduced-order analyses with both closed-form[5-11] and finite element (FE)[12-15] solutions. Reduced-order FE analysis can be further classified into so-called direct[12-14] and indirect[15] stiffness evaluation procedure approaches. For both direct and indirect approaches, the system is first transformed to a reduced set of coupled nonlinear equations, which are solved via numerical integration. Since the eventual application is the analysis and design of practical structures, this paper focuses on developments associated with the indirect approach, which has been implemented for use with commercial finite element codes.[15-17] The previous work[15] using the indirect procedure modeled the dynamic snap-through response with a single transverse mode. However, it has been subsequently shown that a significant improvement can be obtained using a basis consisting of both low-frequency transverse-dominated modes and high-frequency in-plane-dominated modes.[17,18] The present work concentrates on selecting such a basis so that both the transverse and in-plane dynamic behaviors of the system can be accurately modeled.

A clamped-clamped aluminum beam is considered in this work to allow reduced-order analysis results to be compared with a numerically intensive simulation in physical DoF. The dynamic thermal buckling problem is first studied by applying a uniformly distributed, positive temperature increment. The combined thermal-acoustic loading is subsequently investigated through the addition of uniformly distributed acoustic loadings of different intensities. Several response characteristics are investigated including: (i) small amplitude vibration around one of two stable, buckled equilibrium positions, (ii) intermittent snap-through response between the two buckled equilibrium positions, and (iii) persistent snap-through response between the two buckled equilibrium positions. In each case, the reduced-order analysis is performed with two different sets of basis functions, and results are compared with those obtained by numerical simulation in physical DoF.

II. Reduced-Order Numerical Simulation

The reduced-order analysis is first presented as it is used to study the response to both thermal and thermal-acoustic loadings. Similarities between the direct and indirect stiffness evaluation methods are discussed.

A. Modal Coordinate Transformation

In the direct stiffness evaluation approach, the equations of motion for a nonlinear system subjected to a change in temperature can be expressed in the form[12-14]

$$\boldsymbol{M}\ddot{\boldsymbol{X}}(t)+\boldsymbol{C}\dot{\boldsymbol{X}}(t)+\left[K_{\boldsymbol{L}}-K_{\Delta T}(\Delta T)+K_1\left(\boldsymbol{X}(t)\right)+K_2\left(\boldsymbol{X}(t),\boldsymbol{X}(t)\right)\right]\boldsymbol{X}(t)=\boldsymbol{F}(t)+\boldsymbol{F}_{\Delta \boldsymbol{T}} \tag{1}$$

where $\boldsymbol{M}$ is the mass matrix, $\boldsymbol{C}$ is the mass proportional damping matrix (no temperature dependence is assumed), and $K_{\boldsymbol{L}}$, K_1, and K_2 are the linear, quadratic, and cubic stiffness matrices, respectively. $\boldsymbol{X}$ is the displacement response vector and $\boldsymbol{F}$ is the force excitation vector. The thermal effect is present on both sides of Eq. (1); as a change in the linear stiffness matrix $K_{\Delta T}(\Delta T)$ on the left-hand-side, and as a thermal force vector $\boldsymbol{F}_{\Delta \boldsymbol{T}}$ on the right-hand-side.

In the indirect stiffness evaluation approach, the equation of motion is written in the form

$$\boldsymbol{M}\ddot{\boldsymbol{X}}(t)+\boldsymbol{C}\dot{\boldsymbol{X}}(t)+\boldsymbol{F}_{\boldsymbol{NL}}(\boldsymbol{X}(t),\Delta T)=\boldsymbol{F}(t) \tag{2}$$

Here, the thermal effect is represented entirely on the left-hand-side of the equation in the nonlinear restoring force $\boldsymbol{F}_{\boldsymbol{NL}}$, which also contains the linear, quadratic and cubic stiffness terms. Comparing Eqs. (1) and (2), a relationship between direct and indirect formulations is established, namely,

$$\boldsymbol{F}_{\boldsymbol{NL}}(\boldsymbol{X}(t),\Delta T)=\left[K_{\boldsymbol{L}}-K_{\Delta T}(\Delta T)+K_1\left(\boldsymbol{X}(t)\right)+K_2\left(\boldsymbol{X}(t),\boldsymbol{X}(t)\right)\right]\boldsymbol{X}(t)-\boldsymbol{F}_{\Delta \boldsymbol{T}} \tag{3}$$

Continuing with the indirect approach, a set of coupled modal equations with reduced DoF is obtained by applying the modal coordinate transformation $\boldsymbol{X}=\boldsymbol{\Phi q}$ to Eq. (2), where $\boldsymbol{q}$ is the modal displacement response vector. In this study, the set of modal basis functions, $\boldsymbol{\Phi}$, is formed from the linear eigenvalue problem using only that part of the restoring force associated with the linear stiffness, without the effect of temperature. These are sometimes referred to as "cold modes." Generally, a small set of *L* basis functions is included resulting in a modal equation of motion that takes the form

$$\tilde{\boldsymbol{M}}\ddot{\boldsymbol{q}}(t)+\tilde{\boldsymbol{C}}\dot{\boldsymbol{q}}(t)+\tilde{\boldsymbol{F}}_{\boldsymbol{NL}}(q_1(t),q_2(t),\ldots,q_L(t),\Delta T)=\tilde{\boldsymbol{F}}(t) \tag{4}$$

The tilde superscript represents modal quantities, and

$$\tilde{\boldsymbol{M}}=\boldsymbol{\Phi}^T\boldsymbol{M}\boldsymbol{\Phi}=\lceil \boldsymbol{I} \rfloor \qquad \tilde{\boldsymbol{C}}=\boldsymbol{\Phi}^T\boldsymbol{C}\boldsymbol{\Phi}=\lceil 2\zeta_r\omega_r \rfloor \qquad \tilde{\boldsymbol{F}}_{NL}=\boldsymbol{\Phi}^T\boldsymbol{F}_{NL} \qquad \tilde{\boldsymbol{F}}=\boldsymbol{\Phi}^T\boldsymbol{F}\,. \tag{5}$$

B. Indirect Stiffness Evaluation Method

The previously developed[15-17] indirect stiffness evaluation procedure is used. To summarize, the r-th element of the nonlinear restoring force vector in Eq. (4) can be formed by computing

$$\tilde{F}_{NL}^{r}(q_1, q_2, \ldots, q_L, \Delta T) = \sum_{j=1}^{L} d_j^r (\Delta T) q_j + \sum_{j=1}^{L}\sum_{k=j}^{L} a_{jk}^r q_j q_k + \sum_{j=1}^{L}\sum_{k=j}^{L}\sum_{l=k}^{L} b_{jkl}^r q_j q_k q_l \qquad r = 1, 2, \ldots, L \tag{6}$$

where *d*, *a*, and *b* are the linear, quadratic nonlinear, and cubic nonlinear modal stiffness coefficients, respectively. The indirect stiffness evaluation procedure reduces the problem of determining the nonlinear modal stiffness to a series of static nonlinear problems with prescribed displacement fields and, if required, temperatures. The prescribed displacement fields are formed from combinations of modes in the basis. Once the resulting nonlinear forces are determined, the nonlinear modal stiffness coefficients may be found by solution of a simple algebraic system of equations. Note that the thermal loading can have an arbitrary spatial and through-the-thickness distribution, as long as such a distribution is supported by a commercial FE code used to compute the nonlinear restoring forces.

C. Implementation

The program RANSTEP was used to perform the reduced-order analysis with the indirect stiffness evaluation procedure. In particular, the RANSTEP implementation for MSC.NASTRAN was used because of successful application to similar problems.[17] The implementation consists of several steps. The linear eigenvectors are first obtained from a normal modes analysis (Solution 103). The required displacement fields are then formed as a summation of selected and appropriately scaled basis functions. Next, a series of static nonlinear solutions (Solution 106) are performed *at a prescribed elevated temperature* to obtain the corresponding restoring forces. Based on these forces, the modal stiffness coefficients are evaluated. The resulting coupled system of equations, Eq. (4), is numerically integrated using the fourth order Runge-Kutta scheme to obtain a modal displacement time history. An inverse modal transformation allows the physical displacement to be computed.

D. Finite Element Model

The beam under analysis measured 18-in. x 1-in. x 0.09-in (length x width x thickness). The FE model consisted of 144 CBEAM beam elements, each measuring 0.125-in. in length. Clamped boundary conditions were applied at both ends of the beam by specifying zero displacement and rotation. The following material properties were used:

$$E = 10.6 \times 10^6\ psi, \qquad G = 4.0 \times 10^6\ psi, \qquad \rho = 2.588 \times 10^{-4}\ \frac{lb_f - s^2}{in^4}, \qquad \alpha = 12.4\ \frac{\mu - in/in}{^\circ F}.$$

In the analyses that follow, mass proportional damping corresponding to critical damping of 2.0% for the fundamental mode (at 57.8 Hz) was specified.

Displacement results presented later in the paper are in the global coordinate system, which has its origin at the left clamped end of the beam. The *x*-axis coincides with the beam mid-surface and stretches along its span, with the positive *y*-axis pointing upwards. Thus, the in-plane (u) displacement is in the direction of the *x*-axis, and the transverse (v) component in the direction of the *y*-axis.

E. Modal Basis Classification and Selection

It is helpful to categorize the linear eigenvectors that constitute the modal basis by their spatial distribution and by the dominant DoF, e.g. transverse displacement. For the flat, isotropic and symmetric beam structure considered herein, four categories are defined. Those having symmetric transverse displacements are subsequently referred to as symmetric transverse (ST) modes, while those having anti-symmetric transverse displacements are referred to as anti-symmetric transverse (AT) modes. Additionally, those having symmetric in-plane displacements are referred to as symmetric in-plane (SI) modes, while those having anti-symmetric in-plane displacements are referred to as anti-symmetric in-plane (AI) modes. Due to the absence of linear coupling between transverse and in-plane modes for the structure considered, both ST and AT modes have numerically zero in-plane displacement components (u). Similarly, both SI and AI modes have numerically zero transverse displacement components (v). Non-zero rotational DoF (ϕ) are present only in the transverse ST and AT modes. ST modes have an anti-symmetric rotation distribution along the beam span, and AT modes have a symmetric rotation distribution along the beam span. The lowest mode of each of the four categories discussed above is presented in Figure 1. The listing of the first six modes of each category is provided in Table 1. It is seen that the transverse ST and AT modes have lower natural frequencies than the in-plane SI and AI modes.

The most critical task in the reduced-order analysis is the selection of the modal basis, as it dictates the accuracy of the reduced-order solution. It may be intuitive to select a modal basis using characteristics of structural and loading symmetry. For example, for a symmetric planar structure under symmetric transverse loading, a modal basis consisting of only ST modes may suffice. While such intuition may be useful for a linear analysis, it has been demonstrated for both flat[17] and curved[18] structures that such a rationale will lead to an inadequate basis selection for

the nonlinear problem. This is due to coupling in the quadratic and cubic stiffness terms. Therefore, some additional guidance in the form of experimental data, theoretical or numerical analysis, or past reduced-order modeling experience is beneficial.

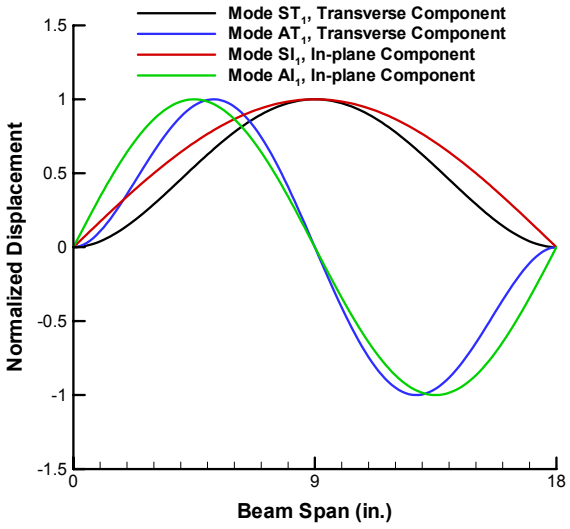

Figure 1: Lowest ST, AT, SI and AI modes of clamped beam.

Table 1: Classification of selected eigenvectors.

Mode Designator	Mode Number	Frequency (Hz)
ST_1	1	57.78
ST_2	3	312.1
ST_3	7	770.1
ST_4	10	1430.6
ST_5	14	2292.5
ST_6	19	3354.3
AI_1	46	11,243
AI_2	81	22,480
AI_3	115	33,706
AI_4	153	44,917
AI_5	221	56,106
AI_6	231	67,268
AT_1	2	159.2
AT_2	4	515.7
AT_3	8	1075.1
AT_4	13	1836.5
AT_5	16	2798.5
AT_6	21	3959.7
SI_1	28	5621.5
SI_2	64	16,802
SI_3	98	28,095
SI_4	133	39,314
SI_5	178	50,514
SI_6	227	61,691

For the beam considered, several factors affected the modal basis selection used in this study. The first factor was earlier experience gained from a reduced-order analysis of symmetric planar structures under symmetric transverse loadings at room temperature ($\Delta T=0$) conditions.[17] In this case, a combination of low-frequency ST modes and high-frequency AI modes was found to compare very well with a numerical simulation in physical DoF. From the study of shallowly curved structures,[18] the additional inclusion of AT and SI modes was required to capture the in-plane behavior associated with autoparametric resonance. The geometry of the curved structure is similar to that of the thermally post-buckled beam, and hence the inclusion of AT and SI modes for the present problem is likely beneficial. Finally, through observations made using results from a numerical simulation analysis in physical DoF to be subsequently presented, significant in-plane motion of the center node was found to

accompany the snap-through response, further substantiating the need for SI modes in the modal basis. While not required for the simple beam, a Proper Orthogonal Decomposition (POD) analysis of data from an FE analysis in physical DoF could provide guidance for more complicated structures.[19,20]

Thus, the modal basis chosen for this study consisted of all four types of modes. Based on the frequency range of the excitation, the six lowest modes of each four types were used to establish the modal basis. In the discussion that follows, this set will be referred to as the 24-mode basis. To explore the impact of selecting an insufficient basis on the quality of the reduced-order results, a truncated basis was assembled from the six lowest ST modes and the six lowest AI modes. This basis lacked the SI modes necessary to capture the in-plane motion at the beam center. In the following, it will be referred to as the 12-mode basis.

F. Modal Stiffness Coefficients

The behavior of modal stiffness coefficients as a function of applied temperature increment was examined and warrants a discussion. For the purpose of this investigation, modal stiffness coefficients were computed at room temperature, and at two uniformly distributed temperature increments of 35°F and 70°F. There was no thermal gradient through the thickness. Since the critical buckling temperature ΔT_{CR} of the beam was found to be 6.6°F, the two elevated temperature cases corresponded to approximately 5.3 and 10.6 times ΔT_{CR}, respectively. Both the 12- and 24-mode bases were used.

Examination of the nonlinear quadratic and cubic modal stiffness matrices revealed that they were not affected by the temperature change. This observation is in agreement with the direct reduced order FE formulation, where the nonlinear stiffness matrices are only a function of displacement, regardless of how this displacement was induced.[13,14] The linear modal stiffness coefficients however were found to be strongly dependent on the temperature change. For the room temperature condition, the linear modal stiffness matrix is uncoupled. The linear stiffness coefficients are the positive eigenvalues and equal to the square of the natural frequencies of the system. Further, since the matrix is diagonal, the linear modal stiffness does not contribute to the overall coupling of transverse and in-plane modes. At elevated temperatures, some of the off-diagonal stiffness terms become significant, resulting in a coupled linear modal stiffness matrix. For both temperatures and bases considered, only the portion of the linear matrix corresponding to the low-frequency transverse modes (ST in the 12-mode basis, and ST and AT in the 24-mode basis) was altered. The off-diagonal terms were symmetric. These observations are also

consistent with the previous direct reduced order FE development.[13,14] Moreover, in the case of the 12-mode basis, the low-frequency portion of the linear stiffness was fully populated, effectively coupling all ST modes included in the basis. In the case of the 24-mode basis, the coupling between ST modes was large, and the coupling between AT modes was large, but no linear cross-coupling occurred between the ST and AT modes. These observations are illustrated in Table 2 with excerpts from the linear modal stiffness matrices computed with the 24-mode basis at different thermal loadings.

Table 2: Selected modal linear stiffness d_{ij} coefficients (x10^6) for the 24-mode basis. Shaded entries indicate cross-coupling between the modes.

ΔT =0°F	ST_1	AT_1	ST_2	AT_2
ST_1	0.132	0	0	0
AT_1	sym	1.001	0	0
ST_2	sym	sym	3.845	0
AT_2	sym	sym	sym	10.50

ΔT =35°F	ST_1	AT_1	ST_2	AT_2
ST_1	-0.543	0	0.534	0
AT_1	sym	-1.524	0	-0.940
ST_2	sym	sym	-1.577	0
AT_2	sym	sym	sym	1.098

ΔT =70°F	ST_1	AT_1	ST_2	AT_2
ST_1	-1.218	0	1.068	0
AT_1	sym	-4.049	0	-1.880
ST_2	sym	sym	-6.998	0
AT_2	sym	sym	sym	-8.303

Another observation from Table 2 is that the linear stiffness coefficients vary linearly with temperature. Relative to the room temperature condition, the change in magnitude of a linear stiffness coefficient computed at a ΔT of 70°F is double that of the value computed at a ΔT of 35°F. Again, this observation is consistent with the direct reduced order FE development and with previous indirect method work.[15] Although this observation is not needed in the process of computing the set of modal stiffness coefficients by the indirect stiffness evaluation method, it may be exploited when temporal temperature variations are required in the analysis. Effectively, it allows a significant computational savings, since only a few linear modal coefficients must be scaled, but not reevaluated, as the temperature changes.

Finally, for the elevated temperature case, the change in sign of the affected diagonal terms from positive to negative provides useful information. Consider a basis consisting of only the first ST mode, so the linear stiffness corresponds to only the 1-1 entry in Table 2. A straight line fit as a function of temperature indicates a change in sign at 6.8°F. Since the first ST mode greatly contributes to the first buckled shape, the temperature at which the sign changes is close to the first critical buckling temperature ΔT_{CR1} of 6.6°F. Similarly, a basis consisting of only

the first AT mode shows a stiffness sign change at 13.9°F, which is close to the second critical buckling temperature ΔT_{CR2} of 13.6°F. As the temperature increases, the number of negative diagonal entries increases. In Table 2 for example, there are three negative diagonal entries at a ΔT of 35°F, and four negative diagonal entries at a ΔT of 70°F.

III. Dynamic Thermal Buckling Analysis

The dynamic response during thermal buckling is of interest because it captures the characteristics of a single snap-through event. The dynamic thermal buckling event was induced by an instantaneous temperature increase of 35°F, uniformly distributed along the length of the beam with a zero through-the-thickness gradient. The beam was initially at rest, with zero displacement and velocity. In the case of the reduced-order analysis, the initial conditions were specified in modal coordinates. A small decaying transverse perturbation force having an initial magnitude of 0.125-lbf was applied at the mid-span node to trigger the stability loss. The force linearly decayed to zero over the period of 0.5s. A fixed integration time step of 1 μs was used for all reduced-order analyses.

A. Physical DoF Analysis

For comparison purposes, the physical DoF analysis was performed using ABAQUS/Explicit. The double precision explicit integration scheme with an automatically determined stable time integration step (referred to as "element by element" in ABAQUS) was utilized for all analyses. The finite element model used was identical to the MSC.NASTRAN-based model used in the RANSTEP reduced-order analysis, except that ABAQUS B21 beam elements were used in place of CBEAM elements. Previous work[17] demonstrated that good comparison can be achieved between reduced order analysis using MSC.NASTRAN and physical simulation in ABAQUS/Explicit.

B. Thermal Buckling Response

The displacement response of the quarter-span and the mid-span nodes is shown in Figure 2 and Figure 3 for the transverse and in-plane components, respectively. At the mid-span location, only the ST modes directly contribute to the transverse response since the AT modes have a node at this location. Similarly only the SI modes directly contribute to the in-plane response at the mid-span location since the AI modes have a node there. The effect of the AT and AI modes is therefore manifested indirectly by altering the system of modal equations. Consequently, modal time histories corresponding to modes ST and AI differ between the 12- and 24-mode bases. In Figure 2, the

24-mode RANSTEP and physical DoF analyses agree quite well, rising from the zero condition with a damped transient response about the final buckling displacement of 0.215-in. for the mid-span location. The 12-mode RANSTEP analysis comes to the same final displacement, but oscillates more toward the positive side of the final displacement. In Figure 3, it is interesting to note that significant in-plane response at the mid-span location is not instantaneous, but is delayed by about 0.05s, clearly indicating the time-varying contribution of the in-plane modes. Since the 12-mode basis lacked the SI modes, this basis was incapable of representing any in-plane behavior at the mid-span location. At the quarter-span location the in-plane transient response characteristic is captured more accurately by the 24-mode basis than by the 12-mode basis, which displays oscillations more toward the negative side of the final displacement. At both locations the damped transient response eventually settles to the zero in-plane displacement associated with the static buckled shape.

Note that a static post-buckling analysis performed with MSC.NASTRAN solution 106 (not shown) yielded nearly identical final buckling displacements. Hence, there are insignificant differences in the manner in which the thermal loading is handled between the NASTRAN-based RANSTEP analysis and the ABAQUS analysis. What is important about the dynamic thermal bucking analysis in this work, however, is not the final at-rest state, but the transient response leading to that state. In this light, the 24-mode basis best captures the relevant dynamics of the single snap-through event. The thermal-acoustic response considered next consists of multiple snap-through events. Therefore, it is expected that the 24-mode basis will also better represent the dynamics than the 12-mode basis.

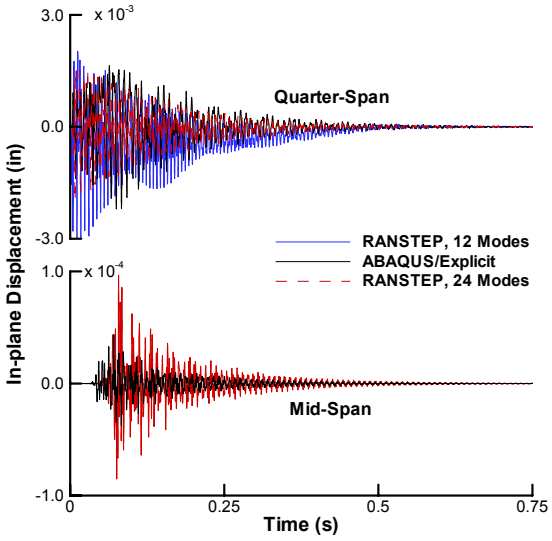

Figure 2: Transverse displacement response of a dynamic thermal buckling event.

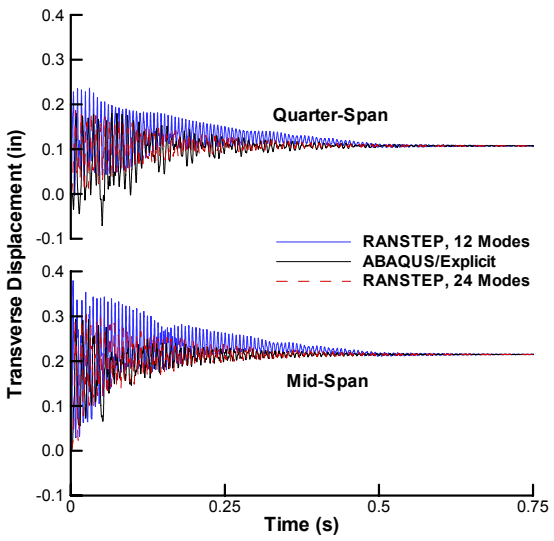

Figure 3: In-plane displacement response of a dynamic thermal buckling event.

IV. Thermal-Acoustic Response Analysis

The dynamic response of the beam to a combined thermal-acoustic load was next investigated. The thermal load was instantaneously applied to the beam via a uniformly distributed temperature increase of 35°F with a zero through-the-thickness gradient. A Gaussian random pressure load with a flat excitation spectrum from 0-1500 Hz was generated using a previously developed procedure.[21] The frequency range of the pressure loading was lower than the maximum frequency of the low frequency ST and AT modes. Almost half of those selected were outside the excitation bandwidth, while all of the SI and AI modes resided significantly above the excitation bandwidth. The pressure was uniformly applied along the span in the transverse direction, irrespective of the deformation, i.e. follower forces were not utilized. Excitation levels of 128 dB, 158 dB, and 170 dB were considered so that different response regimes could be investigated.

The beam was initially at rest, with zero displacement and velocity, in the unbuckled state. A simulated response time history of 2.1384s was performed at each level considered. In the computation of power spectral density (PSD) and probability density function (PDF), five ensembles were averaged. For each ensemble, the initial 0.5*s* was removed to eliminate the start-up transient. In case of the Poincare maps, only a single ensemble with the initial 0.5*s* removed was used for a better clarity of plots. Also, only a single ensemble was utilized to compute the Lyapunov exponents, the computation of which was based on the algorithm offered by Wolf et al.[22]

A. Thermal-Acoustic Response

The three response regimes are illustrated with ABAQUS/Explicit-generated transverse displacement time histories of the mid-span node in Figure 4. The regimes can be characterized as: (i) small amplitude vibration around one of the two stable buckling equilibrium positions (128 dB), (ii) intermittent snap-through response between the two buckling equilibrium positions (158 dB), and (iii) persistent snap-through response between the two equilibrium positions (170 dB).

The PSD of the mid-span transverse displacement response at 128 dB is shown in Figure 5. Since the time histories from which these were generated lacked the initial thermal-buckling transient, the results from the 12- and 24-mode bases compare equally well with the physical DoF simulation. A significant static displacement component due to thermal buckling is apparent. The corresponding Poincare map and the PDF exhibiting a Gaussian distribution with a non-zero mean are shown in Figure 6. With the initial thermal-buckling transient removed, the

in-plane displacement response was negligible at this location. The Lyapunov exponent computed for this case converged to a negative value, indicating that a chaotic response was not induced.

When the excitation level is increased such that intermittent snap-through response occurs, differences between the 12- and 24-mode bases become apparent. Figure 7 shows the PSD of the mid-span transverse displacement response at 158 dB. Very good agreement is noted between the 24-mode and physical DOF analyses across the frequency range. The 12-mode reduced-order analysis however exhibits amplification at some peaks. All three analyses reflect the dominant zero-frequency component. The in-plane response is shown in Figure 8. Again, the 24-mode solution captured all of the essential features of the physical response. The 12-mode solution is unable to produce any in-plane displacement response due to the lack of SI modes in the basis.

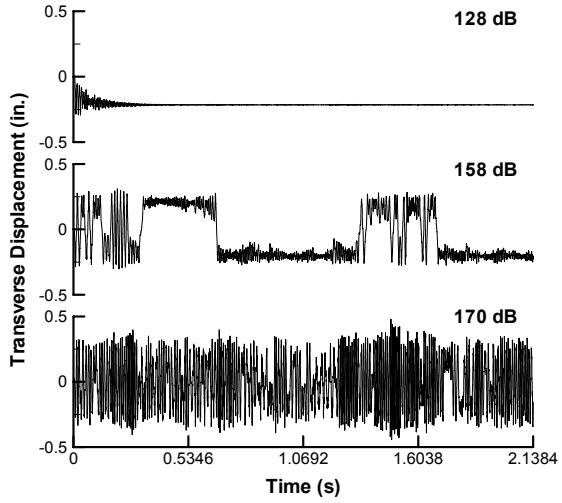

Figure 4: Transverse displacement response at 35ºF and 128, 158, and 170 dB excitations.

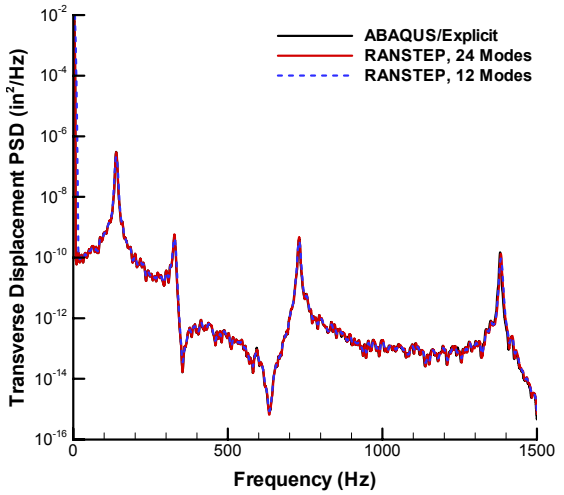

Figure 5: Mid-span transverse displacement response PSD at 35ºF and 128 dB.

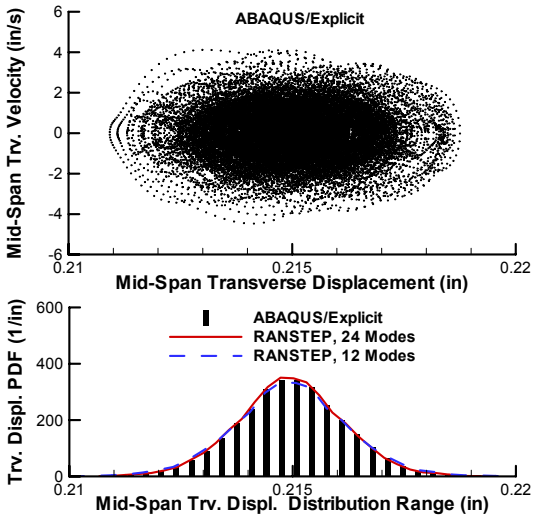

Figure 6: Transverse displacement Poincare map and PDF at 35°F and 158 dB.

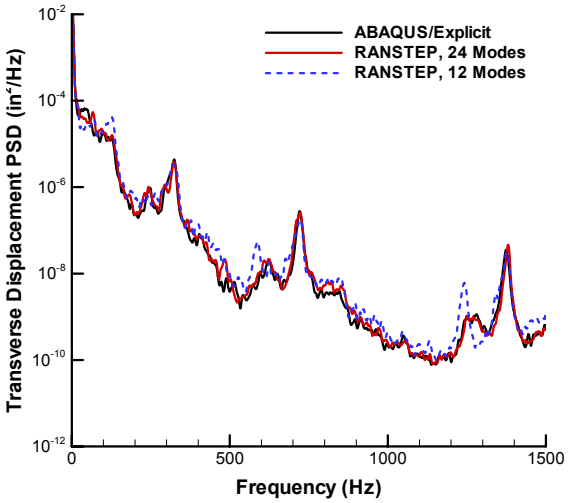

Figure 7: Mid-span transverse displacement response PSD at 35°F and 158 dB.

The transverse displacement Poincare map and the PDF at the mid-span are shown in Figure 9. Based on these two representations it is clear that the majority of vibration cycles at this level occurred about either of the two thermally buckled equilibrium positions. In particular, for the simulation period considered, the structure happened to spend more time oscillating about the lower equilibrium position. This is also consistent with the 158 dB time history response presented in Figure 4. Small values of the probability density in the proximity of the zero distribution range, Figure 9, indicate the few instances when the response snapped between the two equilibrium positions. The Lyapunov exponent computed for the mid-span transverse displacement showed a positive value, indicative of chaotic motion. Due to intermittent snap-thorough, however, its temporal convergence was not achieved.

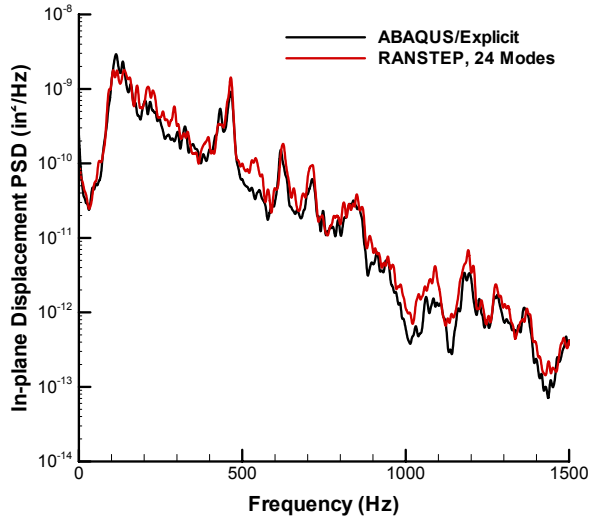

Figure 8: Mid-span in-plane displacement response PSD at 35°F and 158 dB.

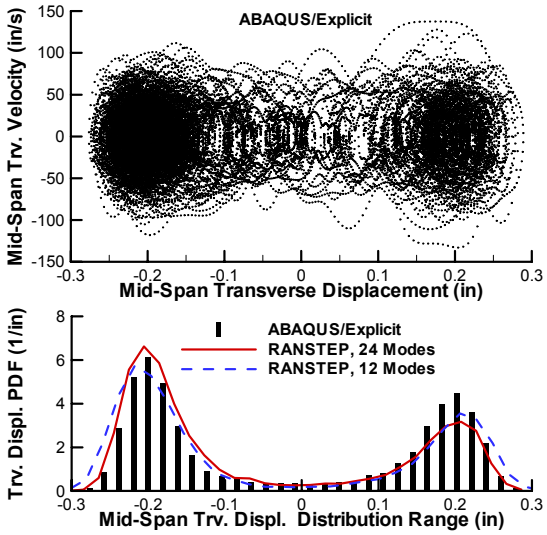

Figure 9: Transverse displacement Poincare map and PDF at 35°F and 158 dB.

It is often advantageous to observe the behavior at more than one location on the structure to help further identify liabilities and limitations associated with modal reduction. The quarter-span location was selected for this purpose, as the dynamic displacement response there exhibits significant in-plane and transverse components. The quarter-span transverse displacement response PSD at the 158 dB excitation level is shown in Figure 10. Like the mid-span response in Figure 7, the 24-mode solution compares favorably with the physical DoF solution across the frequency range. Above 1 kHz, 12-mode solution misses one peak and amplifies another. Again, the dominant zero-frequency component is seen. The quarter-span in-plane displacement PSD is shown in Figure 11. The 24-mode solution

again compares favorably with the physical DoF solution across the frequency range, while the 12-mode solution poorly matched the physical response in the low and high-frequency ranges.

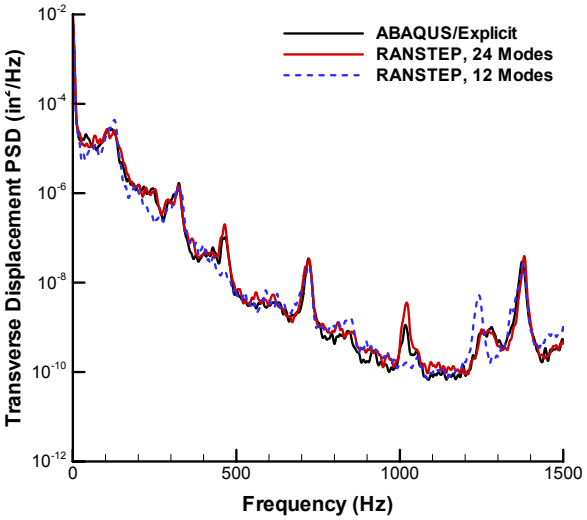

Figure 10: Quarter-span transverse displacement response PSD at 35°F and 158 dB.

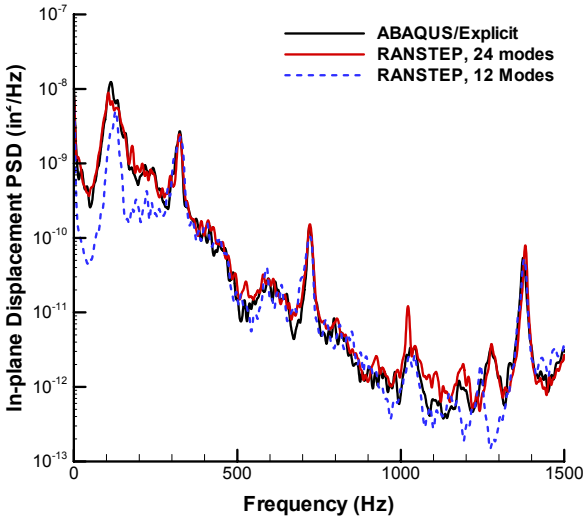

Figure 11: Quarter-span in-plane displacement response PSD at 35°F and 158 dB.

To help better understand how these differences manifest themselves, and what their origins are, one can observe the contribution of various modal displacement components. Plotted in Figure 12 are the lowest components of each mode type (ST_1, AT_1, SI_1, and AI_1) for the 24-mode reduced-order solution at 35°F and 158 dB. Also plotted are the reduced-order in-plane and transverse displacement time histories obtained from the inverse modal transformation at the quarter-span location. The modal responses from modes ST_1 and AT_1 are on the order of 10^{-3}, while those from the SI_1 and AI_1 modes are two orders of magnitude smaller. Mode ST_1 is strongly correlated with the transverse physical displacement (v). The correlation coefficient has a value of -0.92. Similarly, mode AI_1 is strongly correlated with the in-plane physical displacement (u), with the correlation coefficient of -0.83. For both correlation coefficients the negative signs originate from a normalization of the ST_1 and the AI_1 eigenvector to a negative value.

Of most interest in Figure 12 are modes SI_1 and AT_1, which are not included in the 12-mode basis. These modes exhibit similar behavior to that of the decaying in-plane transient response of the single dynamic thermal buckling event, first seen in Figure 3. Unlike the mid-span location, both modes directly contribute to the response at the quarter-span location. A significant increase in the SI_1 and AT_1 modal responses occur at every snap-through event.

Hence these modes play an important role in the response during such events, and further indicate that the 12-mode basis is insufficient for accurately capturing the snap-through response.

The mid-span transverse and in-plane displacement response PSDs, obtained at a ΔT of 35°F and at the 170 dB excitation level, are presented in Figure 13 and Figure 14, respectively. This excitation level was shown in Figure 4 to result in a persistent snap-through response. Both 24-mode PSDs compare very well with the physical DOF solution. As expected, the transverse response PSD from the 12-mode solution compares less favorably, and does not exist for the in-plane response. Because of the persistent snap-through response, the transverse static component was no longer dominant, as shown in Figure 13. The transverse displacement Poincare map and PDF for this loading condition are shown in Figure 15. Here it is shown that as the intensity of snap-through is increased, the rate of the zero-crossings increases. Hence, the center part of the PDF distribution fills in compared to the intermittent snap-through conditions. The PDF obtained with the 24-mode basis matches the PDF distribution obtained from the physical DoF analysis better than the 12-mode solution. The 12-mode solution reveals too broad a distribution range and generally tends to underestimate the probability density. The Lyapunov exponent computed at this excitation level was positive, and a good temporal convergence was achieved. Consequently, the response can be regarded as being chaotic.

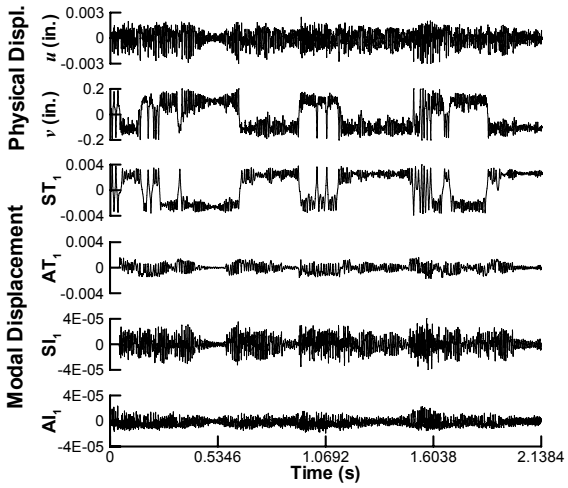

Figure 12: Quarter-span physical and modal displacement response at 35°F and 158 dB.

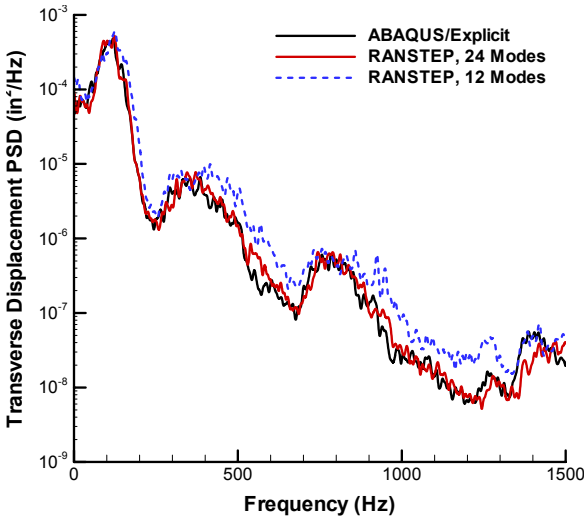

Figure 13: Mid-span transverse displacement response PSD response at 35°F and 170 dB.

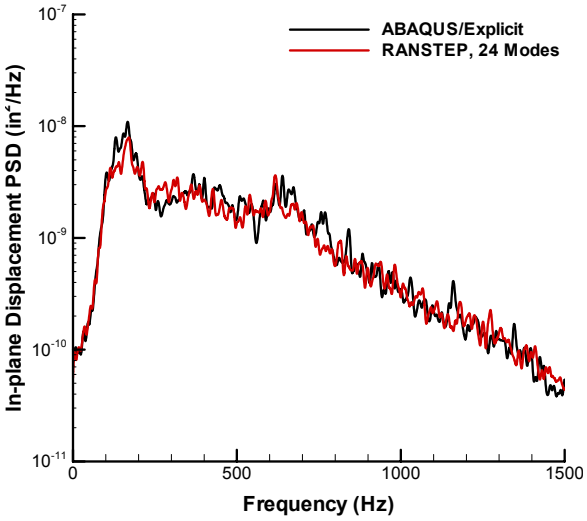

Figure 14: Mid-span in-plane displacement response PSD at 35F and 170dB.

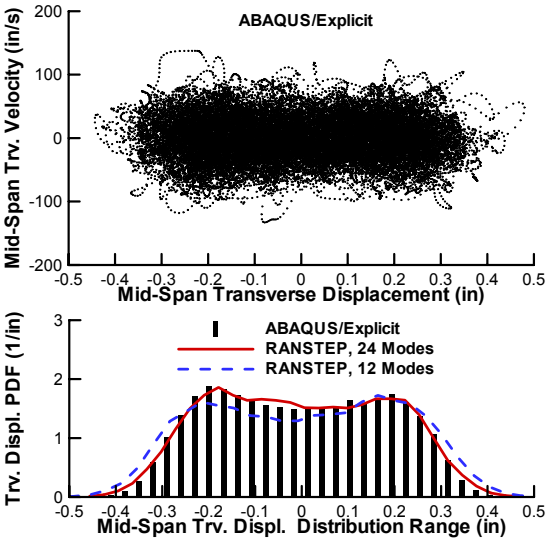

Figure 15: Mid-span transverse displacement Poincare map and PDF at 35F and 170dB.

Finally, for a fixed temperature increment of 35°F, the number of transverse displacement zero-crossings is presented as a function of the random pressure excitation level. Having good agreement in the number of crossings is of interest because large excursions associated with snap-through will significantly influence the fatigue life. It is seen in Figure 16 that snap-through does not occur up to a random pressure level of about 152 dB (0.1152 psi). Then, beginning in the range between 152 dB and 158 dB (0.2304 psi), the snap-through behavior is initiated and the number of zero-crossings starts growing as the excitation level is further increased. Results obtained in physical DoF and by the reduced-order analysis utilizing 24-mode reduction are in a good agreement despite the relatively short simulation time studied. Thus, the suitability of the reduced order analysis for subsequent fatigue studies is further established.

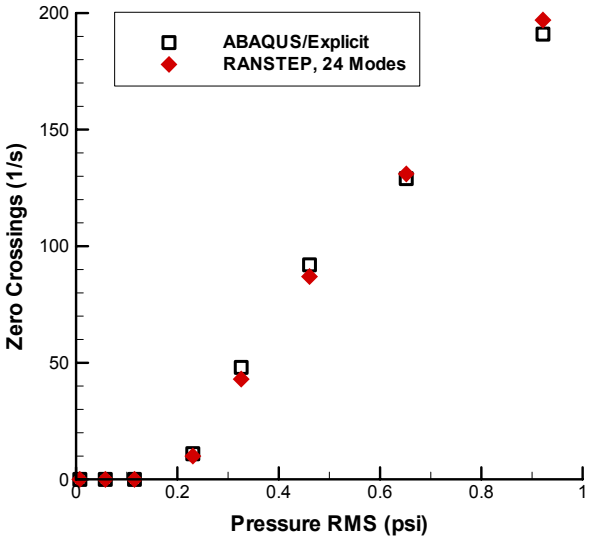

Figure 16: Transverse displacement zero-crossing intensity at 35F.

V. Conclusion

A reduced-order FE based method for predicting thermo-acoustic random response in a nonlinear regime was presented. Two sets of modal bases were examined in the study, and the corresponding reduced-order analysis results were compared with solutions obtained with an analysis in physical DoF.

The effect of elevated temperature on the modal stiffness coefficients was first examined. It was found that only the linear stiffness coefficients corresponding to low-frequency transverse displacement modes were affected by the temperature change. These stiffness coefficients were found to vary linearly with temperature. Quadratic and cubic stiffness coefficients were unaffected. As a result, a computational benefit may be gained for problems with a time-varying thermal loading magnitude because linear coefficients need only be scaled.

In the analysis of dynamic thermal buckling and thermal-acoustic response, it was found that a modal basis consisting of four types of modes (ST, AT, SI and AI) more accurately predicted the response than a basis consisting of only ST and AI modes. In particular, for both loading conditions, the contribution of SI and AT modes becomes more significant as the structure transitions to a different equilibrium position.

Although not in scope of this study, the fatigue life will be affected in a different manner depending on the response regime. For the response about one of the thermally buckled equilibrium positions, a significant mean stress component will be introduced. The mean stress has been shown to adversely affect the fatigue life.[23,24] Additionally, for intermittent and persistent snap-through, large cyclic stress amplitudes will rapidly accumulate and lead to a shorter fatigue life. Therefore, a continuation of this study to address stress recovery and fatigue estimation is deemed to be worthwhile.

References

[1]Pozefsky, P., Blevins, R.D., and Langanelli, A.L., "Thermal-vibro-acoustic loads and fatigue of hypersonic flight vehicle structure," Wright Labs, Wright Patterson Air Force Base AFWAL-TR-89-3014, 1989.

[2]Istenes, R.R., Rizzi, S.A., and Wolfe, H.F., "Experimental nonlinear random vibration results of thermally buckled composite panels," *Proceedings of the 36th AIAA/ASME/ASCE/AHS/ASC Structures, Structural Dynamics and Materials Conference*, AIAA-95-1345-CP, New Orleans, LA, 1995, pp. 1559-1568.

[3]Murphy, K.D., Virgin, L.N., and Rizzi, S.A., "Experimental snap-through boundaries for acoustically excited, thermally buckled plates," *Experimental Mechanics*, Vol. 36, No. 4, 1996, pp. 312-317.

[4]Ng, C.F. and Clevenson, S.A., "High-intensity acoustic tests of a thermally stressed plate," *Journal of Aircraft*, Vol. 28, No. 4, 1991, pp. 275-281.

[5]Lee, J., "Displacement and strain histograms of thermally buckled composite plates in random vibration," *Proceedings of the 37th AIAA/ASME/ASCE/AHS/ASC Structures, Structural Dynamics, and Materials Conference*, AIAA-96-1347, Salt Lake City, UT, 1996.

[6]Lee, J., "Displacement and strain statistics of thermally buckled plates," *Journal of Aircraft*, Vol. 38, No. 1, 2001, pp. 104-110.

[7]Lee, J., Vaicaitis, R., Wentz, K., Clay, C., Anselmo, E., and Crumbacher, R., "Predicition of statistical dynamics of thermally buckled composite plates," *Proceedings of the 39th AIAA/ASME/ASCE/AHS/ASC Structures, Structural Dynamics, and Materials Conference*, AIAA-98-1975, Long Beach, CA, 1998.

[8]Ng, C.F., "Nonlinear and snap-through response of curved panels to intense acoustic excitation," *Journal of Aircraft*, Vol. 26, No. 3, 1989, pp. 281-288.

[9]Ng, C.F. and Wentz, K.R., "The prediction and measurement of thermoelastic response of plate structures," *Proceedings of the 31st AIAA/ASME/ASCE/AHS/ASC Structures, Structural Dynamics, and Materials Conferece*, AIAA-1990-988, Long Beach, CA, 1990.

[10]Ghazarian, N. and Locke, J., "Nonlinear random response of antisymmetric angle-ply laminates under thermal-acoustic loading," *Journal of Sound and Vibration*, Vol. 186, No. 2, 1995, pp. 291-309.

[11]Maekawa, S., "On the sonic fatigue life estimation of skin structures at room and elevated temperatures," *Journal of Sound and Vibration*, Vol. 80, No. 1, 1982, pp. 41-59.

[12]Duan, B., Mei, C., and Ro, J.J., "Nonlinear response of thermal protection system at supersonic speeds," *Proceedings of the 42nd AIAA/ASME/ASCE/AHS/ASC Structures, Structural Dynamics, and Materials Conference*, AIAA-2001-1659, Seattle, WA, 2001.

[13]Guo, X., Przekop, A., and Mei, C., "Nonlinear random response of shallow shells at elevated temperatures using finite element modal method," *Proceedings of the 45the AIAA/ASME/ASCE/AHS/ASC Structures, Structural Dynamics and Materials Conference*, AIAA-2004-1558, Palm Springs, CA, 2004.

[14]Mei, C., Dhainaut, J.M., Duan, B., Spottswood, S.M., and Wolfe, H.F., "Nonlinear random response of composite panels in an elevated thermal environment," Air Force Research Laboratory AFRL-VA-WP-TR-2000-3049, Wright-Patterson Air Force Base, OH, October 2000.

[15]Mignolet, M.P., Radu, A.G., and Gao, X., "Validation of reduced order modeling for the prediction of the response and fatigue life of panels subjected to thermo-acoustic effects," *Structural Dynamics: Recent Advances, Proceedings of the 8th International Conference*, The Institute of Sound and Vibration Research, University of Southampton, Southampton, UK, 2003, M.J. Brennan, M.A. Ferman, B.A.T. Petersson, S.A. Rizzi, and K. Wentz (ed.).

[16]Muravyov, A.A. and Rizzi, S.A., "Determination of nonlinear stiffness with application to random vibration of geometrically nonlinear structures," *Computers and Structures*, Vol. 81, No. 15, 2003, pp. 1513-1523.

[17]Rizzi, S.A. and Przekop, A., "The effect of basis selection on static and random acoustic response using a nonlinear modal simulation," NASA Langley Research Center NASA/TP-2005-213943, Hampton, VA December 2005.

[18]Przekop, A. and Rizzi, S.A., "Nonlinear reduced order finite element analysis of structures with shallow curvature," *AIAA Journal*, in press, 2006.

[19]Feeny, B.F., "On proper orthogonal co-ordinates as indicators of modal activity," *Journal of Sound and Vibration*, Vol. 255, No. 5, 2002, pp. 805-817.

[20]Feeny, B.F. and Kappagantu, R., "On the physical interpretation of proper orthogonal modes in vibrations " *Journal of Sound and Vibration*, Vol. 211, No. 4, 1998, pp. 607-616.

[21]Rizzi, S.A. and Muravyov, A.A., "Comparison of nonlinear random response using equivalent linearization and numerical simulation," *Structural Dynamics: Recent Advances, Proceedings of the 7th International Conference*, Vol. 2, The Institute of Sound and Vibration Research, University of Southampton, Southampton, UK, 2000, N.S. Ferguson, H.F. Wolfe, M.A. Ferman, and S.A. Rizzi (ed.), pp. 833-846.

[22]Wolf, A., Swift, J.B., Swinney, H.L., and Vastano, J.A., "Determining Lyapunov exponents from a time series," *Physica*, Vol. 16D, No. 1985, pp. 285-317.

[23]Rizzi, S.A. and Przekop, A., "Estimation of sonic fatigue by reduced-order finite element based analysis," *Structural Dynamics: Recent Advances*, *Proceedings of the 9th International Conference*, The Institute of Sound and Vibration Research, University of Southampton, Southampton, UK, 2006, M.J. Brennan, B.R. Mace, J.M. Muggleton, B.A.T. Petersson, K.D. Murphy, S.A. Rizzi, and R. Shen (ed.).

[24]Sweitzer, K.A. and Ferguson, N.S., "Mean stress effects on random fatigue of nonlinear structures," *Proceedings of the XII International Congress on Sound and Vibration*, Lisbon, Portugal, 2005.